**International Journal of Power Electronics and Drive System (IJPEDS)**
Vol. 17, No. 2, June 2026, pp. 1288~1303
ISSN: 2088-8694, DOI: 10.11591/ijpeds.v17.i2.pp1288-1303 

# Design simulation and analysis of an MPPT technique using ANN integral backstepping and SMC for PV systems

**Naoufal Zhani, Hassane Mahmoudi**
Department of Electrical Engineering, Mohammadia School of Engineers, Mohammed V University in Rabat, Rabat, Morocco

**Article Info**

***Article history:***

Received Jul 24, 2025
Revised Feb 9, 2026
Accepted Feb 21, 2026

***Keywords:***

Artificial neural networks
Sliding mode control
Boost converter
Integral backstepping
MATLAB/Simulink
Maximum power point tracking
Photovoltaic system

**ABSTRACT**

This paper introduces the design of an innovative hybrid MPPT method called artificial neural networks-integral backstepping sliding mode control (ANN-IBSMC). This approach combines artificial neural networks (ANNs), which output the maximum power point voltage using inputs such as irradiance and temperature, with a robust control strategy. The designed controller aims to track the reference voltage with high accuracy and responsiveness by modifying the pulse width modulation of the DC-DC converter in the photovoltaic system. The IBSMC integrates the advantages of two control methods: the stability and accuracy of integral backstepping, and the robustness and fast response of sliding mode control (SMC). This combination enables improved precision, high convergence speed, enhanced robustness, and strong stability, the latter being ensured by the Lyapunov function. To evaluate the performance of the proposed controller, a comparative study is performed against other hybrid control techniques, such as the ANN-backstepping controller, the ANN-integral sliding mode controller, and the ANN-backstepping sliding mode controller, using MATLAB/ Simulink. A sensitivity and robustness analysis was carried out.



***Corresponding Author:***

Naoufal Zhani
Department of Electrical Engineering, Mohammadia School of Engineers
Mohammed V University in Rabat
Rabat, Morocco
Email: zhani.naoufal@research.emi.ac.ma

## 1. INTRODUCTION

The worldwide demand for energy continues its rapid growth, driven by the expansion in large-scale industrial production. However, the use of fossil fuels poses a major threat to humanity and the ecosystems of our planet. Addressing this challenge necessitates replacing these polluting energy sources with renewable energies to combat global warming. Against this backdrop, optimizing energy production from renewable energy sources has become a primary objective for researchers specializing in control systems and energy efficiency. The maximum utilization of solar energy through photovoltaic (PV) panels has seen significant advancements. However, electrical generation based on solar input depends heavily on variations in irradiance and temperature, making energy yield optimization a complex task. To maximize electrical output, the system's operating point must remain at the maximum power point (MPP). This requires regulating the converter so that the PV module's voltage consistently matches the MPP voltage, regardless of meteorological variations.

Numerous researchers have developed and studied various control techniques to track and maintain the MPP under changing weather conditions. Key performance criteria include convergence speed, accuracy, stability, and robustness, all of which are crucial for optimal utilization of this inexhaustible energy source. several studies [1], [2] have proposed early maximum power point tracking (MPPT) techniques based on conventional approaches such as perturb & observe (P&O) and hill-climbing. Other studies [3], [4] have focused on the incremental conductance method, while additional strategies relying on open-circuit voltage and

fractional short-circuit current have also been investigated. However, these conventional methods exhibit significant limitations, leading to an inherent trade-off between tracking speed, accuracy, and system stability.

To overcome these limitations, several studies [5], [6] have developed controllers based on advanced approaches, such as sliding mode control (SMC) and backstepping, to enhance the operational performance of PV systems. Sliding mode control is characterized by high robustness and fast convergence under varying climatic conditions but suffers from the chattering phenomenon, which may degrade system stability. In contrast, the backstepping control ensures high stability and tracking precision based on Lyapunov theory, at the cost of increased design complexity and sensitivity to parameter uncertainties. Additionally, intelligent MPPT techniques, such as those based on fuzzy logic [7], particle swarm optimization (PSO), or artificial neural networks (ANN) [8], have emerged. Several studies [9], [10] have shown that fuzzy logic exhibits good adaptive stability, although it offers limited precision strongly dependent on predefined rules. Other works [11], [12] have demonstrated that the PSO algorithm ensures fast and stable convergence toward the global maximum power point but may produce slight residual oscillations if parameters are not properly tuned. Other studies based on ANN methods [13], [14] have highlighted their high accuracy and rapid response due to learning capabilities, although robustness may decrease outside the trained operating domain. Recently, hybrid controllers combining conventional, intelligent, and advanced approaches have been proposed, including backstepping–P&O, ANN–backstepping, and ANN–sliding mode controllers. These hybrid techniques aim to simultaneously enhance stability, robustness, and tracking speed of the MPP. For instance, the backstepping–P&O controller provides a good compromise between speed and stability, though it remains less accurate under rapid irradiance variations. Previous studies [15], [16] have shown that ANN–backstepping offers high precision and stability but with a slightly slower convergence time. Similarly, other works [17], [18] have demonstrated that ANN–SMC combines the robustness of SMC with the predictive capability of ANN, while still presenting residual chattering issues. Each technique presents its own advantages and limitations, imposing an inevitable trade-off between speed, precision, robustness, and stability. Consequently, current research trends focus on the development of advanced control strategies capable of reducing, or even eliminating, this trade-off inherent to the performance of photovoltaic systems.

This study proposes a new integrated control strategy, referred to as the artificial neural networks–integral backstepping sliding mode controller (ANN–IBSMC). This hybrid approach coherently combines artificial intelligence with advanced nonlinear control by leveraging the predictive capability of the artificial neural network, the stability and accuracy provided by the integral backstepping method [19], [20], and the robustness and fast response of SMC [21], [22]. The overall stability of the system is ensured by the Lyapunov function, making this synergy an effective way to unify the strengths of each control method. The ANN generates a reference voltage $V_{REF}$ corresponding to the maximum available power for each meteorological variation. The main novel contribution of this method lies in its ability to simultaneously reduce the trade-off between speed, accuracy, robustness, and stability, thereby outperforming previously reported hybrid techniques such as ANN–backstepping [23]-[25], ANN–ISMC [26], [27], and ANN–BSMC [28]. The performance of the ANN–IBSMC controller has been evaluated and compared under various weather conditions using MATLAB/Simulink, demonstrating rapid convergence, high accuracy, and enhanced robustness. A sensitivity and robustness study of this controller has been carried out.

## 2. MODELLING OF THE PHOTOVOLTAIC SYSTEM

The photovoltaic system consists of a solar panel and a DC-DC boost converter, with a load connected at the output, as shown in Figure 1. In the proposed controller, the artificial neural network generates the system's reference voltage in real time according to the irradiance and temperature experienced by the photovoltaic panel. The integral backstepping sliding mode control (IBSMC) then applies the control law to the MOSFET to track this reference voltage and ensure efficient power transfer to the load.

### 2.1. Modelling of PV module

The primary element in a solar module is the solar cell. Figure 2 shows the equivalent electrical schematic for the solar cell. Where $I\_ph$ is the photocurrent, I_$out$ the output current, and $I\_sat$ the saturation current. $V\_out$ denotes the output voltage, with $R\_s$ and $R\_sh$ representing series and shunt resistances. Constants like Boltzmann's constant $k$, the ideality factor $a$, temperature $T$, and electron charge $q$ are also involved. Temperature effects are accounted for using K_i, dT, and $K\_v$ . Solar irradiance is represented by $G$ and its nominal value $G\_n$, while I_cc and $V\_oc$ stand for short-circuit current and open-circuit voltage, respectively.

$$Iout = Iph - Isat\left(e^{\frac{q(Vout+(Iout*Rs))}{a*k*T}} - 1\right) - \frac{Vout+Iout*\mathrm{Rs}}{R_{sh}} \quad (1)$$

With:

$$I_{ph} = (I_{cc} + K_i * dT) * \frac{G}{G_n} \quad (2)$$

$$I_{sat} = \frac{Icc+Ki*dT}{e^{\frac{q*(Voc+(Kv*dT))}{a*k*T}}-1} \quad (3)$$

The photovoltaic module used in the simulation has a maximum power (Pmax) of 240 W, achieved at a voltage of 30.05 V (Vmp) and a current of 7.99 A (Imp). Its open-circuit voltage (Voc) is 37.58 V, while the short-circuit current (Isc) reaches 8.49 A. The temperature coefficient of the short-circuit current (Ki) is 0.15 mA/°C. The module consists of 60 cells (Ns).

Figure 3 illustrates the power-voltage characteristics of the photovoltaic module for different irradiances (1 kW/m², 0.7 kW/m², and 0.5 kW/m² at a temperature of 25 °C) and different temperatures (25 °C, 30 °C, and 50 °C at an irradiances of 1 kW/m²), with the maximum power point varying according to these meteorological conditions. Therefore, for each variation in these two inputs, a specific voltage will correspond to the maximum power point. For optimal and efficient conversion, the system's operating point must be set at the maximum power point for each variation in meteorological conditions.

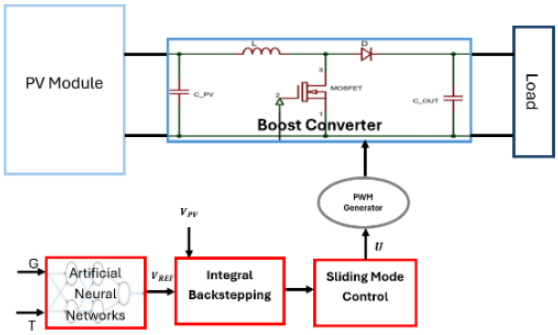


Figure 1. System PV

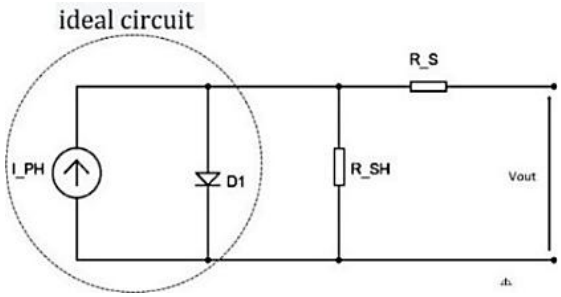


Figure 2. Electrical representation of a PV solar cell

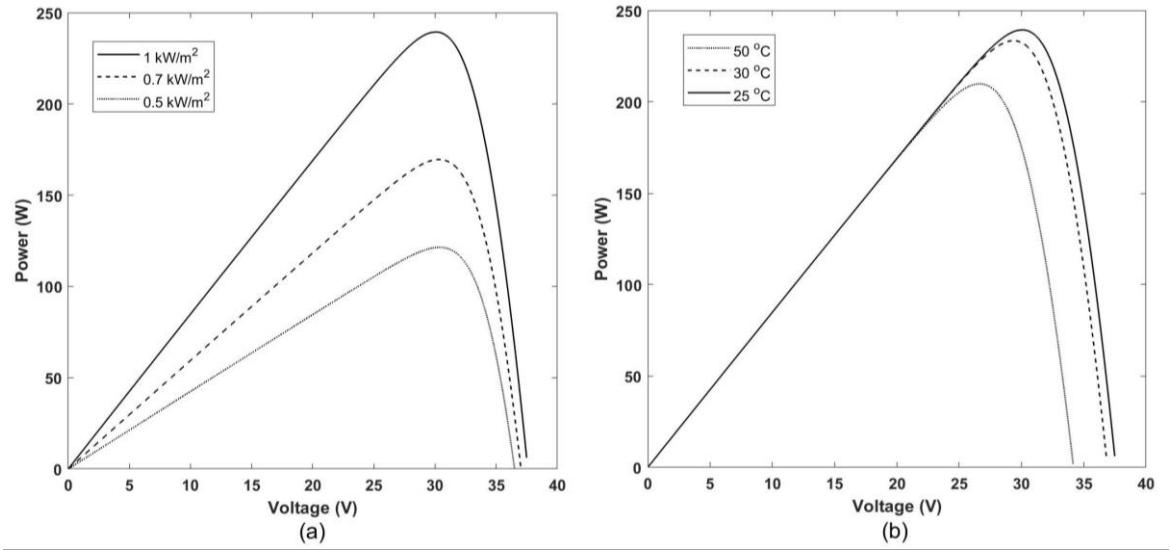


Figure 3. Power-voltage characteristic: (a) under varying irradiance levels and (b) at various temperatures

### 2.2. Modeling of DC-DC converter boost converter

The DC-DC converter alters the amplitude of the input voltage, either decreasing or increasing it, or performing both actions based on the system's output requirements, as described in [29], [30]. The study

focuses on the boost converter, as shown in Figure 4, which increases the PV voltage to a value three times higher at the output, typically around 100 V, depending on the weather conditions. This amplitude change is achieved by varying the converter's duty cycle through the applied control technique.

By applying Kirchhoff's voltage laws during the boost DC-DC converter's on and off intervals of the MOSFET transistor, we obtain (4).

$$\begin{cases} \dot{V}_{PV} = \frac{1}{C_{PV}} I_{PV} - \frac{1}{C_{PV}} I_L \\ \dot{I}_L = \frac{1}{L} V_{PV} - \frac{1}{L}(1-U) V_{OUT} \\ \dot{V}_{OUT} = \frac{1}{C_{OUT}}(1-U) I_L - \frac{1}{C_{OUT}} I_{OUT} \end{cases} \quad (4)$$

The voltage across the photovoltaic module is represented by $V_{PV}$, the voltage at the converter's output by $V_{OUT}$, the current generated by the PV module, denoted $I_{PV}$, output current by $I_{OUT}$, and the current flowing through the inductor by $I_L$. The MOSFET's duty cycle is represented by $U$, and the output capacitor, input capacitor, and inductance are represented by $C_{OUT}$, $C_{PV}$ and $L$, respectively.

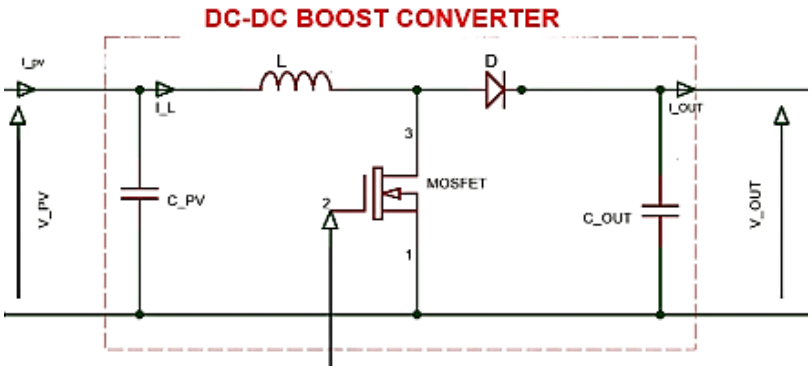


Figure 4. Electrical diagram of the boost converter

## 3. CONTROL OF THE SYSTEM

The proposed approach is based on the combination of the ANN and the IBSMC for controlling the photovoltaic system. The ANN, with its predictive and adaptive capabilities, can provide real-time estimates of the system's uncertainties and nonlinearities. The IBSMC controller is designed to use these estimates to achieve precise tracking of the reference voltage while maintaining robustness and fast response against disturbances and meteorological variations. This synergy will combine the strengths of each technique, leveraging the adaptability and predictive capability of the ANN together with the precision and robustness of the IBSMC, providing a promising framework for effective and stable control.

### 3.1. Artificial neural networks

Previous studies [31], [32] have described that an ANN, inspired by the functioning of biological neurons, links inputs to outputs through mathematical equations. The efficiency of the network mainly depends on the quality of the database, the number of hidden layers, and the adopted learning algorithm. In this work, the training process was carried out using 80 input cases, with irradiance ranging from 100 to 1000 W/m² and temperature varying between 5 °C and 60 °C. The ANN generates a reference voltage $V_{REF}$ corresponding to the maximum power point voltage $V_{MPP}$. The designed architecture consists of an input layer (irradiance, temperature), one hidden layer with 50 neurons, and an output layer that presents the desired voltage. The Bayesian regularization algorithm was adopted to ensure good generalization, even with noisy inputs.

Figure 5 illustrates the training performance of the artificial neural network. The training error decreases rapidly during the first iterations and stabilizes after approximately 100 epochs. The best performance is achieved at epoch 810, with a mean squared error of $7.02 \times 10^{-6}$. The relatively small gap between the training and testing curves indicates that the model does not suffer from overfitting and retains strong generalization ability. These results confirm the stability and reliability of the ANN training process, ensuring accurate estimation of the nonlinear parameters of the photovoltaic system over a wide range of operating conditions. The minimal deviation observed confirms the strong generalization capability of the network on unseen data. Figure 6 shows the correlation between the ANN-predicted outputs and the target

values. The three plots correspond respectively to the training, testing, and overall datasets. In all cases, the correlation coefficient R reaches 1, indicating a very strong agreement between predicted and actual targets. This high accuracy demonstrates that the ANN effectively learned the nonlinear relationship between the photovoltaic system input parameters and the maximum power point.

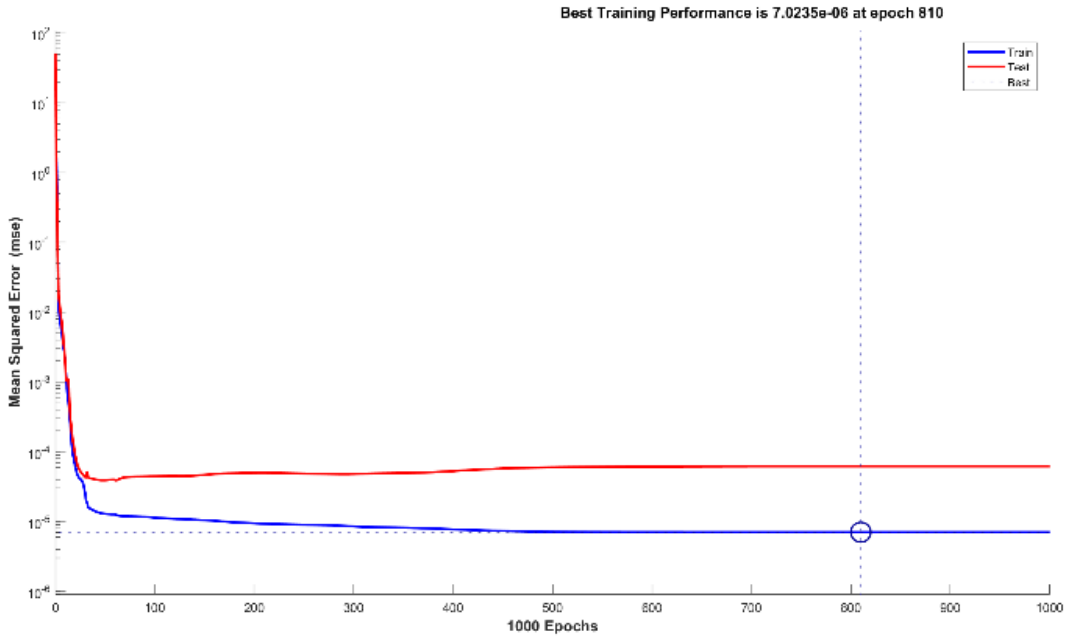


Figure 5. Performances of the ANN

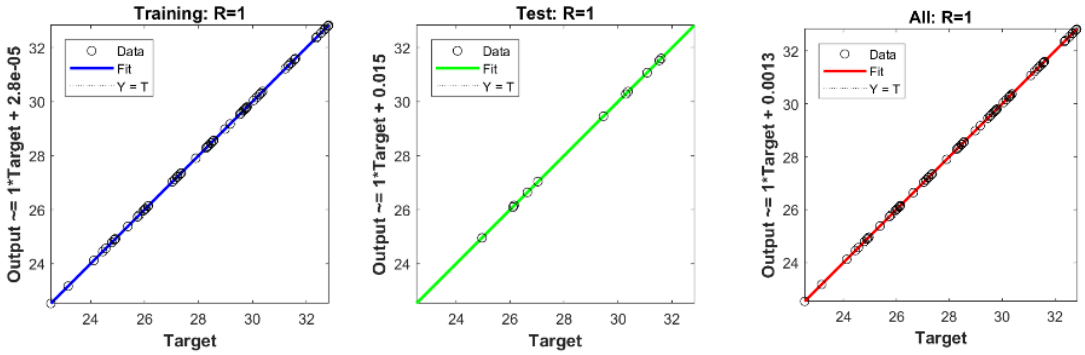


Figure 6. Performances and regression of ANN

### 3.2. Artificial neural networks-integral backstepping sliding mode control

The ANN–IBSMC is a hybrid MPPT approach that combines the artificial neural network with a a control structure consisting of backstepping with its integral action, and SMC. The overall system stability ensured by the Lyapunov function, whose derivative remains strictly negative, thereby guaranteeing error convergence and stability against external disturbances and parametric uncertainties. The modeling of this technique is presented as (5).

$$\begin{cases} \dot{V}_{PV} = \frac{1}{C_{PV}} I_{PV} - \frac{1}{C_{PV}} I_L \\ \dot{I}_L = \frac{1}{L} V_{PV} - \frac{1}{L}(1-U) V_{OUT} \end{cases} \quad (5)$$

The voltage tracking error between $V_{PV}$ and $V_{REF}$ is defined by (6).

$$\varepsilon_1 = V_{PV} - V_{REF} \quad (6)$$

The derivative with regard to the time of $\varepsilon_1$ is given by (7).

$$\dot{\varepsilon}_1 = \dot{V}_{PV} - \dot{V}_{REF} = \frac{1}{C_{PV}} I_{PV} - \frac{1}{C_{PV}} I_L - \dot{V}_{REF} \quad (7)$$

The integral action error added to the control low as (8).

$$e_1 = \varepsilon_1 + \zeta \quad (8)$$

With the integral function is defined by (9).

$$\zeta = K \int (V_{PV} - V_{REF}) \quad (9)$$

The first Lyapunov candidate function as (10).

$$V_1 = \frac{1}{2} {\varepsilon_1}^2 + \frac{1}{2} K \zeta^2 \quad (10)$$

The derivative of (10) is (11).

$$\dot{V}_1 = \varepsilon_1 \dot{\varepsilon_1} + K \zeta \dot{\zeta} = \varepsilon_1 \left( \frac{1}{C_{PV}} I_{PV} - \frac{1}{C_{PV}} I_L - \dot{V}_{REF} + K \zeta \right) \quad (11)$$

In the case that $\dot{V}_1$ is negative with $K_1 > 0$, we have (12).

$$\frac{1}{C_{PV}} I_{PV} - \frac{1}{C_{PV}} I_L - \dot{V}_{REF} + K \zeta = -K_1 \varepsilon_1 \quad (12)$$

Based on (12), the reference inductor current controller can be derived as (13) ($\alpha_1 = I_{L\_ref}$).

$$\frac{1}{C_{PV}} I_{PV} - \frac{1}{C_{PV}} \alpha_1 - \dot{V}_{REF} + K \zeta = -K_1 \varepsilon_1 \quad (13)$$

$$\alpha_1 = C_{PV} (K_1 \varepsilon_1 - \dot{V}_{REF} + K \zeta) + I_{PV} \quad (14)$$

The derivative of (14) is (15).

$$\dot{\alpha}_1 = C_{PV} (K_1 \dot{\varepsilon}_1 - \ddot{V}_{REF} + K \dot{\zeta}) + \dot{I}_{PV} \quad (15)$$

Step 2: In this step, the controller output from the first step $\alpha_1$ is selected as the control variable. A second error signal is then defined.

$$\varepsilon_2 = I_L - \alpha_1 \quad (16)$$

The (11) and (12) become respectively (17) and (18).

$$\dot{V}_1 = \varepsilon_1 \left( \frac{1}{C_{PV}} I_{PV} - \frac{1}{C_{PV}} (\varepsilon_2 + \alpha_1) - \dot{V}_{REF} + K \zeta \right) \quad (17)$$

$$\frac{1}{C_{PV}} I_{PV} - \frac{1}{C_{PV}} (\varepsilon_2 + \alpha_1) - \dot{V}_{REF} + K \zeta = -K_1 \varepsilon_1 - \frac{\varepsilon_2}{C_{PV}} \quad (18)$$

The sliding surface is given by $s = \varepsilon_2$ the derivative of (16) is (19).

$$\dot{s} = \dot{\varepsilon}_2 = \dot{I}_L - \dot{\alpha}_1 = \frac{1}{L} V_{PV} - \frac{1}{L} (1 - U) V_{OUT} - (C_{PV} (K_1 \dot{\varepsilon}_1 - \ddot{V}_{REF} + K \dot{\zeta}) + \dot{I}_{PV}) \quad (19)$$

To guarantee the convergence of the two errors, the second Lyapunov function is selected as (20).

$$V_2 = V_1 + \frac{1}{2} s^2 \quad (20)$$

The derivative of (20) is (21).

$$\dot{V}_2 = \dot{V}_1 + s\dot{s} = -K_1{\varepsilon_1}^2 + s\left(-\frac{\varepsilon_1}{C_{PV}} + \dot{s}\right) \tag{21}$$

Selecting the exponential reaching law expressed as (22).

$$-\frac{\varepsilon_1}{C_{PV}} + \dot{s} = -C_3\big(C_1 s + C_2 Sign(s)\big) \tag{22}$$

Replacing $\dot{s}$ in (22) with its expression from (19), we obtain (23).

$$\begin{aligned} &-\frac{\varepsilon_1}{C_{PV}} + \frac{1}{L}V_{PV} - \frac{1}{L}(1-U)V_{OUT} - (C_{PV}(K_1\left(-K_1\varepsilon_1 - \frac{s}{C_{PV}}\right) - \ddot{V}_{REF} + K\varepsilon_1) + \dot{I}_{PV}) \\ &= -C_3(C_1 s + C_2 Sign(s)) \end{aligned} \tag{23}$$

The expression for the control input determined as (24).

$$U_{IBSMC} = 1 + \frac{L}{V_{OUT}}\left(C_3\big(C_1 s + C_2 Sign(s)\big) + C_{PV}\left(K\varepsilon_1 - \ddot{V}_{REF} + K_1\left(-\frac{s}{C_{PV}} - K_1\varepsilon_1\right)\right) + \dot{I}_{PV} + \frac{\varepsilon_1}{C_{PV}} - \frac{V_{PV}}{L}\right) \tag{24}$$

Replacing (21) with its expression from (22), we obtain (25).

$$\dot{V}_2 = -K_1{\varepsilon_1}^2 - C_3 s\big(C_1 s + C_2 Sign(s)\big) < 0 \tag{25}$$

With $C_1, C_2\ and\ C_3$ should be positive. This ensures the asymptotic convergence of $\varepsilon_1$ and $\varepsilon_2$ to zero, which in turn guarantees the convergence of $V_{PV}$ toward $V_{REF}$.

To evaluate the performance of the proposed controller, a comparative study is conducted with other hybrid control approaches. Three main combinations are considered, ANN–backstepping as in (26), proposed in [23]–[25], which combines the adaptive capabilities of the ANN with the stability of classical backstepping; ANN–ISMC (28) proposed in [26], [27], which integrates the ANN with the robustness of integral SMC; and finally, ANN–BSMC (30) proposed in [28], which combines both the stability of backstepping and the robustness of SMC with the ANN. This comparison illustrates how the combination of different techniques can leverage the specific advantages of each method and highlights the effectiveness of the IBSMC for controlling the photovoltaic system.

$$U_{BACKSTEPPING} = 1 - \frac{1}{V_{OUT}}\left(V_{PV} - L\dot{\alpha}_1 - L\left(\frac{\varepsilon_1}{C_{PV}} - K_2\varepsilon_2\right)\right) \tag{26}$$

With

$$\begin{cases} \varepsilon_1 = V_{PV} - V_{REF} \\ \varepsilon_2 = I_L - \alpha_1 \\ \alpha_1 = I_{PV} + C_{PV}\big(K_1\varepsilon_1 - \dot{V}_{REF}\big) \end{cases} \tag{27}$$

$$U_{INTEGRAL\ SMC} = 1 - \frac{L}{V_{OUT}}\left(\frac{V_{PV}}{L} - \dot{I}_{PV} + C_{PV}\big(-K_3 sign(\sigma) + \ddot{V}_{REF} - \lambda\dot{\varepsilon}_1 + K_4\varepsilon_1\big)\right) \tag{28}$$

With

$$\begin{cases} \varepsilon_1 = V_{PV} - V_{REF} \\ \sigma = \lambda\varepsilon_1 + \dot{\varepsilon}_1 + K_4\int\varepsilon_1 \\ \dot{\sigma} = \lambda\dot{\varepsilon}_1 + \ddot{\varepsilon}_1 + K_4\varepsilon_1 = -K_3 sign(\sigma) \end{cases} \tag{29}$$

$$U_{BSMC} = 1 - \frac{1}{g_1}\left(-\frac{\varepsilon_1}{C_{PV}} + f_1 - C_{PV}K_1\left(-\frac{s}{C_{PV}} - K_1\varepsilon_1\right) - F\frac{\partial V_{PV}}{\partial t} + g_1\big(C_1 s + C_2 Sign(s)\big)\right) + C_{PV}\frac{\partial^2 V_{ref}}{\partial t} \tag{30}$$

$$g_1 = \frac{V_{OUT}}{L}\ f_1 = \frac{V_{PV}}{L}\ F = \frac{\partial I_{PV}}{\partial V_{PV}}$$

The simulation of the proposed photovoltaic system was carried out using MATLAB/Simulink. The entire system, including the photovoltaic generator and the DC–DC converter, was fully implemented in this environment, as illustrated in Figure 7. The simulation was performed using the ode45 solver with a discrete

time step of $1\times10^{-6}$ s to ensure high precision of the results. The PV module has the characteristics mentioned above in the modelling section. The energy conversion stage is based on a DC–DC boost converter. The converter parameters are defined as follows: the input capacitor $C_{PV}$ = 4700 nF, the inductor L = 0.35 mH, the output capacitor $C_{OUT}$ = 220 nF, switching frequency F = 5 kHz, IGBT, and diode. The structure of the proposed controller, shown in Figure 8, is defined by (24) and (25). The controller parameters were set to K = 12000, $K_1$ = 700000, $C_1$ = 0.00001, $C_2$ = 2000, and $C_3$ = 50. These values were obtained through iterative simulation-based tuning to ensure system stability, fast dynamic response, and accurate maximum power point tracking.

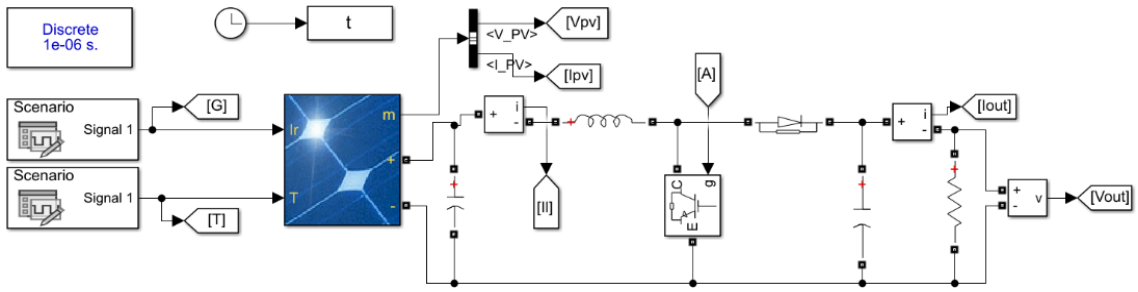


Figure 7. PV system model simulation

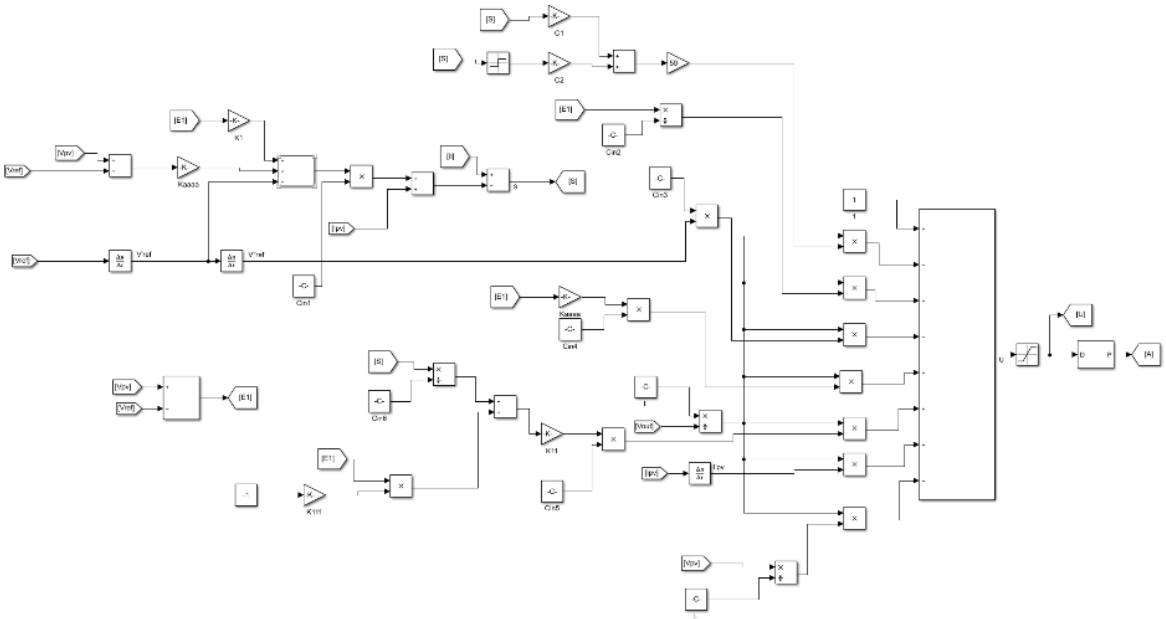

Figure 8. Proposed controller IBSMC in MATLAB Simulink

## 4. RESULTS AND DISCUSSION

To evaluate the robustness of the proposed control strategy, the photovoltaic system was subjected to variable meteorological conditions, including changes in solar irradiance and temperature, as shown in Figure 9. These variations were as follows: 1000 W/m² and 30 °C from 0 s to 0.9 s; 500 W/m² and 30 °C from 0.9 s to 1.5 s; 500 W/m² and 10 °C from 1.5 s to 1.6 s; 700 W/m² and 10 °C from 1.6 s to 2 s; 700 W/m² and 25 °C from 2 s to 2.2 s; and 950 W/m² and 25 °C from 2.2 s to 3 s. These variations were applied directly to the photovoltaic model during the 3-second simulation.

Figure 10 illustrates the reference voltage $V_{REF}$ generated by the artificial neural network presented above, as well as the voltage of the PV module controlled by the proposed technique, the ANN–IBSMC. The voltage of the PV module using the proposed technique, shown in Figure 10, follows the reference voltage generated by the artificial neural network under different meteorological conditions, with high accuracy, fast convergence, remarkable stability, and strong robustness.

To thoroughly evaluate the performance of the proposed controller, a comparative study of this technique with other techniques proposed in the literature has been explored, such as the hybrid technique ANN-backstepping proposed in [23]–[25], the hybrid technique ANN-ISMC proposed in [26], [27], and finally, the hybrid technique ANN-BSMC proposed in [28]. These four techniques are simulated in MATLAB/Simulink, controlling boost DC-DC converters with the same dimensioning, connected to photovoltaic modules with the same characteristics. The same meteorological conditions from Figure 9 are applied to these four PV systems. The reference voltage generated by the ANN is transmitted to all four control techniques.

Figure 11 illustrates the voltages of the four PV modules and the reference voltage. The proposed method demonstrates excellent accuracy in tracking the reference voltage under different changes in temperature and irradiance. The speed of convergence of the photovoltaic voltage using the proposed method was remarkable during both the rise and fall of the reference voltage. Additionally, the proposed method's stability and robustness are highly satisfactory throughout the simulation period. Figures 12 and 13, respectively, represent the current of the PV module and the error between the PV module voltage and the reference voltage. The convergence speed of the proposed method towards the appropriate current value for the MPP voltage is impressive, and its stability is remarkable. The error epsilon1 of the proposed method quickly converges to zero, practically canceling out, unlike the other techniques, which leave a very small gap between the epsilon1 curve and zero. This gap varies between 0.005 and 0.03, depending on the technique applied to the PV system.

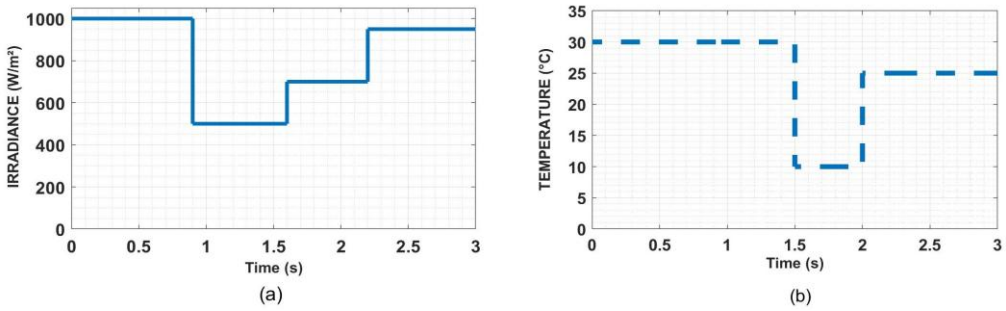


Figure 9. Weather conditions: (a) irradiance and (b) temperature

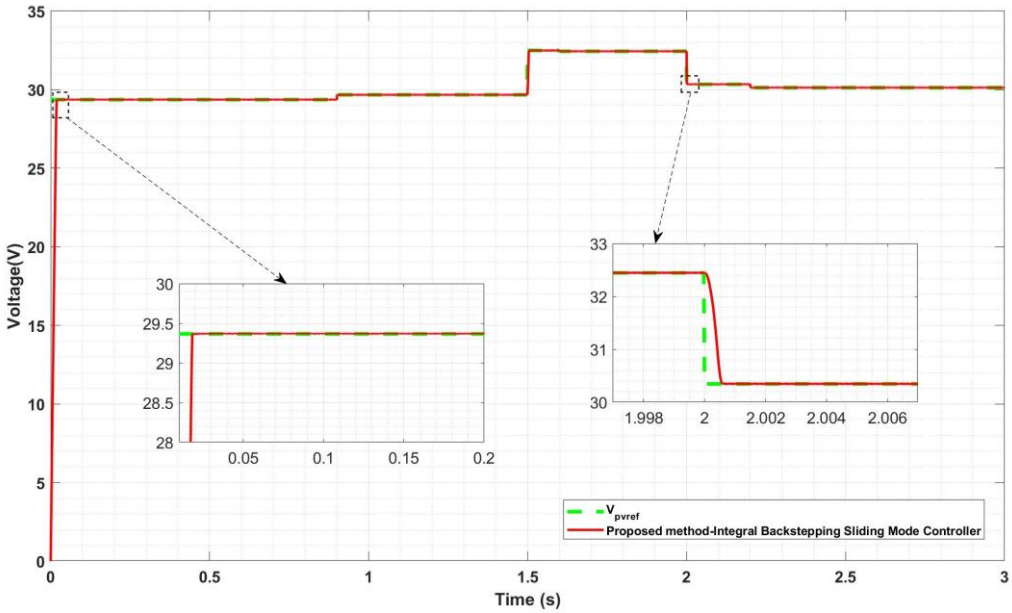


Figure 10. Photovoltaic voltage

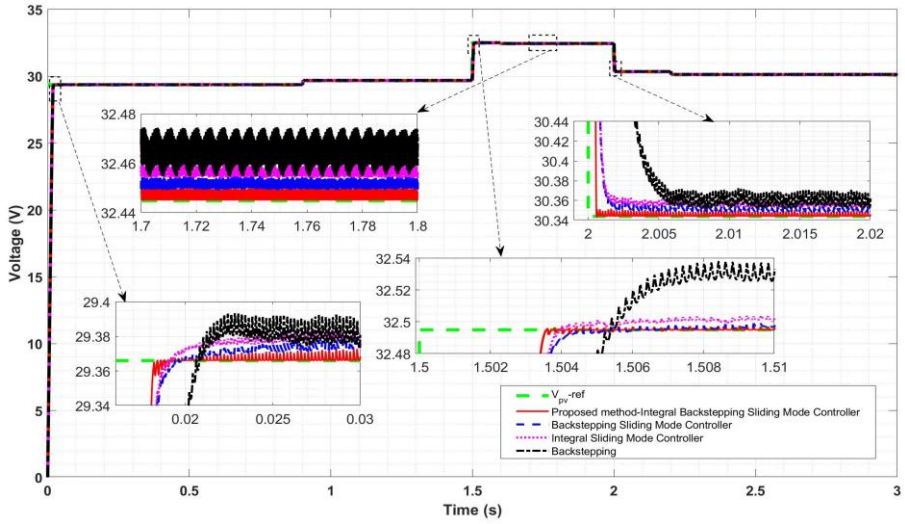


Figure 11. Photovoltaic voltage

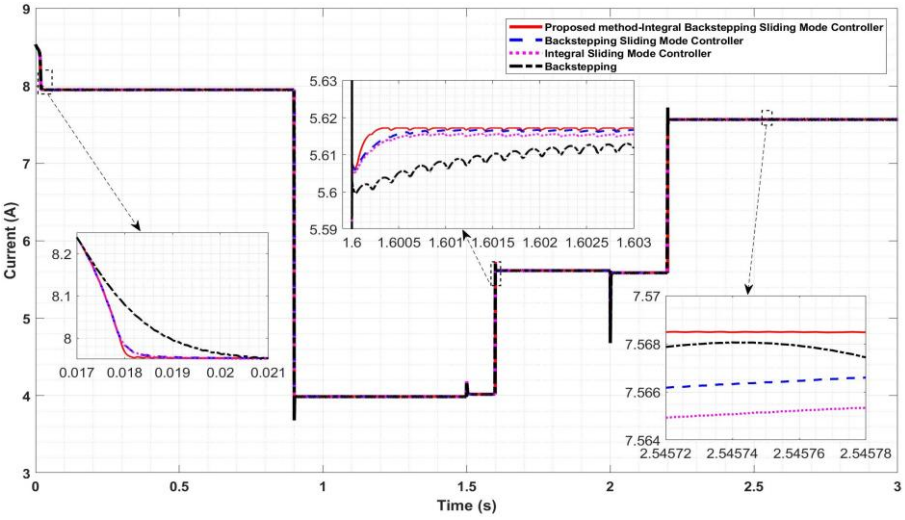


Figure 12. Photovoltaic current

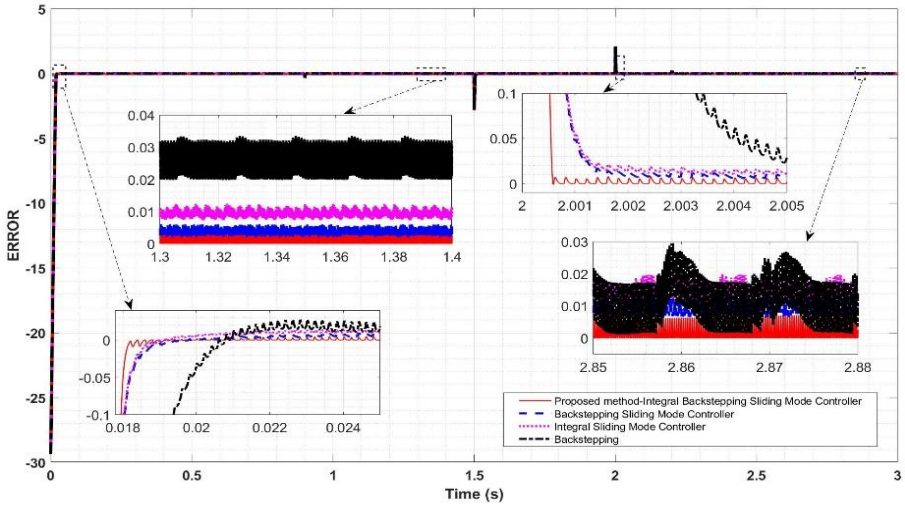


Figure 13. Epsilon

Table 1, extracted from Figures 11–13, analytically presents the performance of the voltage and current of the photovoltaic module, as well as the median of the error $\varepsilon_1$, representing the deviation between the desired and actual voltage of the photovoltaic module, and its accuracy percentage. The voltage of the proposed algorithm is the closest to the reference voltage among all the compared techniques. The IBSMC method achieves the lowest median error of $1.04\times10^{-4}$, with an accuracy rate of 99.996%, outperforming BSMC (99.976%), ISMC (99.961%), and backstepping (99.901%). Although these percentage differences may seem small, they are significant in photovoltaic systems, where slight voltage deviations can cause considerable power loss. This low error indicates that, for most of the simulation time, the error remains very close to zero, reflecting efficient and stable tracking of the reference voltage. The analysis of the voltage and current ripples presented in the table shows that the IBSMC algorithm provides the lowest voltage and current ripples among all compared methods. For example, the voltage ripple varies between 2.2 mV and 5.9 mV, while the current ripple remains below 1.7 mA, which is significantly lower than in other methods. These low ripples result in a significant reduction of stress on the converter components, particularly on capacitors and inductors, thereby extending their lifespan and improving the overall system reliability. In comparison, the conventional backstepping and integral sliding mode techniques exhibit slightly higher ripples, which could impose additional stress on the converter and affect long-term stability. Thus, the choice of IBSMC not only ensures precise tracking of the maximum power point, achieving 99.996%, but also enhances signal quality and reduces switching stress, which is crucial for applications where durability and energy efficiency of the PV system are priorities. These results highlight the superiority of the IBSMC technique, particularly in terms of the accuracy of tracking the reference value compared to the other techniques considered.

Figure 14 shows the power of the PV module. The proposed method demonstrates a very high convergence speed towards the maximum power point for each variation in meteorological conditions compared to the other simulated techniques. This also results in a very good gain, which is due to the high accuracy in tracking and maintaining the reference voltage. Table 2 presents a comparison of the energy yield and the convergence time of the power for each variation of the meteorological conditions. The data are extracted from Figure 14. The power obtained by the IBSMC strategy exceeds that of the other techniques by a few milliwatts, and its convergence time is significantly faster in all scenarios, outperforming the other methods. This responsiveness demonstrates the controller's ability to efficiently adapt to sudden changes in irradiance and temperature, ensuring high efficiency and optimal extraction of maximum power at all times. The percentage improvements of IBSMC compared to the other methods are calculated based on the average convergence time over the six steps. IBSMC is found to be 8.30% faster than BSMC and 10.31% faster than ISMC on average, while the backstepping method is significantly slower, with a convergence time 61.75% longer than IBSMC. These figures highlight the overall superior dynamic performance of the IBSMC strategy across varying environmental conditions.

Table 1. The performance of the voltage and current of the photovoltaic module

| Atmospheric conditions | G (W/m²)<br>T (°C) | 1000<br>30 | 500<br>30 | 500<br>10 | 700<br>10 | 700<br>25 | 950<br>25 |
|---|---|---|---|---|---|---|---|
| V_ref | Referntiel Voltage (V) | 29.366 | 29.675 | 32.495 | 32.445 | 30.344 | 30.13 |
| Backstepping | V_pv (V) | 29.38 | 29.7 | 32.525 | 32.465 | 30.36 | 30.14 |
| | Voltage ripple (mV) | 17 | 11 | 10.4 | 14 | 13 | 16 |
| | I_pv (A) | 7.949 | 3.986 | 4.018 | 5.6138 | 5.585 | 7.565 |
| | Current ripple (mA) | 4.5 | 1.6 | 1.5 | 2 | 2.2 | 4 |
| | Error of tracking | $1{,}562\,.\,10^{-2}$ | | | | | |
| | Accuracy rate (%) | 99.901% | | | | | |
| Integral sliding mode controller | V_pv (V) | 29.38 | 29.685 | 32.504 | 32.456 | 30.355 | 30.145 |
| | Voltage ripple (mV) | 4.2 | 2.5 | 3.3 | 3.7 | 4.4 | 6.5 |
| | I_pv (A) | 7.949 | 3.9884 | 4.0186 | 5.6152 | 5.5865 | 7.565 |
| | Current ripple (mA) | 1.6 | 0.4 | 0.4 | 0.8 | 0.8 | 1.3 |
| | Error of tracking | $1{,}282\,.\,10^{-2}$ | | | | | |
| | Accuracy rate (%) | 99.961% | | | | | |
| Backstepping sliding mode controller | V_pv (V) | 29.375 | 29.679 | 32.499 | 32.452 | 30.35 | 30.14 |
| | Voltage ripple (mV) | 5.5 | 2.5 | 3 | 4.2 | 4.7 | 6 |
| | I_pv (A) | 7.9505 | 3.9892 | 4.0194 | 5.616 | 5.5872 | 7.566 |
| | Current ripple (mA) | 1.7 | 0.4 | 0.4 | 0.8 | 0.9 | 1.5 |
| | Error of tracking | $1{,}678\,.\,10^{-3}$ | | | | | |
| | Accuracy rate (%) | 99.976% | | | | | |
| Integral backstepping sliding mode controller | V_pv (V) | 29.367 | 29.676 | 32.496 | 32.447 | 30.345 | 30.131 |
| | Voltage ripple (mV) | 4.2 | 2.2 | 2.5 | 4 | 4 | 5.5 |
| | I_pv (A) | 7.953 | 3.9897 | 4.0197 | 5.617 | 5.5882 | 7.568 |
| | Current ripple (mA) | 1.7 | 0.4 | 0.4 | 0.8 | 0.8 | 1.3 |
| | Error of tracking | $1{,}04\,.\,10^{-4}$ | | | | | |
| | Accuracy rate (%) | 99.996% | | | | | |

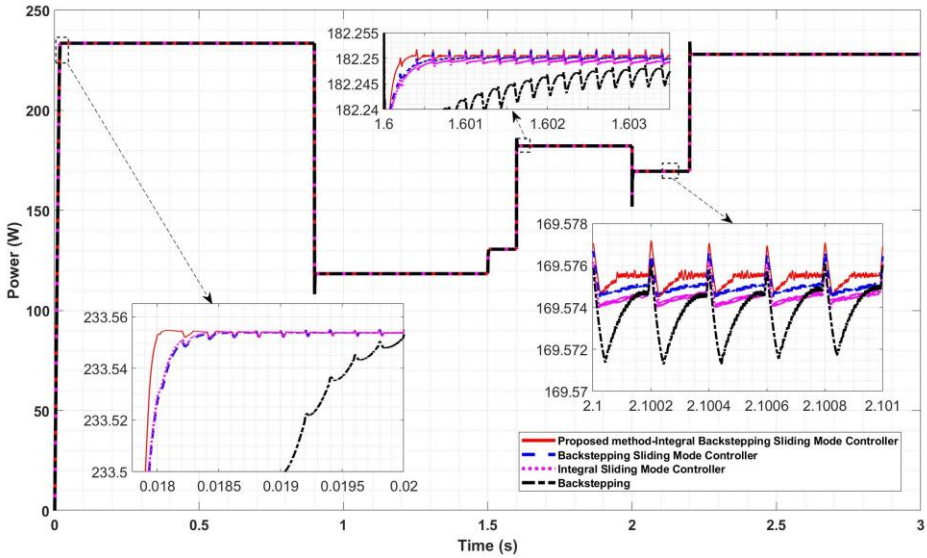


Figure 14. Photovoltaic power

Table 2. Energy yield and the convergence time of the power for each variation of the meteorological conditions

| Atmospheric conditions | G (W/m²) T (°C) | 1000 30 | 500 30 | 500 10 | 700 10 | 700 25 | 950 25 |
|---|---|---|---|---|---|---|---|
| Backstepping | P_pv (W) | 233.552 | 118.3955 | 130.622 | 182.249 | 169.574 | 228.036 |
| | Ripple (mW) | 6.6 | 2.3 | 2.68 | 4.65 | 4.52 | 10.4 |
| | Tracking time (ms) | 20.5 | 1,6 | 5 | 25 | 5.8 | 2.4 |
| Integral sliding mode controller | P_pv (W) | 233.552 | 118.3975 | 130.6233 | 182.2493 | 169.5745 | 228.0365 |
| | Ripple (mW) | 3.5 | 1.4 | 1.57 | 2.4 | 2.18 | 3.7 |
| | Tracking time (ms) | 18,5 | 0,4 | 3.6 | 0.7 | 1.6 | 0.9 |
| Backstepping sliding mode controller | P_pv (W) | 233.553 | 118.3985 | 130.6235 | 182.2497 | 169.575 | 228.0375 |
| | Ripple (mW) | 3.2 | 1.38 | 1.35 | 2.2 | 2.2 | 3.9 |
| | Tracking time (ms) | 18.5 | 0,4 | 3.6 | 0.6 | 1.4 | 0.8 |
| Integral backstepping sliding mode controller | P_pv (W) | 233.554 | 118.3988 | 130.6236 | 182.2505 | 169.5755 | 228.039 |
| | Ripple (mW) | 3.2 | 1.38 | 1.35 | 2.3 | 2.2 | 3.8 |
| | Tracking time (ms) | 18 | 0.35 | 3.4 | 0.3 | 0.6 | 0.4 |

To analyze the sensitivity and robustness of this controller, three sets of simulations were conducted: to study the impact of slight changes in controller parameters, the presence of input disturbances, and the gradual degradation of components. Figure 15 shows the PV voltage and power under ±5% variation of the controller parameters. The voltage takes about 2 ms longer to reach the reference value when the parameters are decreased by 5%, while an increase of 5% causes an overshoot of 30 mV. The PV power also exhibits slightly increased ripples. Figure 16 illustrates the PV voltage and power in the presence of input disturbances, corresponding to inaccuracies in the voltage and current sensors. Disturbances of 1% to 5% cause a deviation of 250 mV for 1% disturbances and up to 400 mV with unwanted ripples for 5% disturbances during rapid changes in weather conditions. This variation affects the generated power by 0.076% for 1% disturbances and 0.13% for 5% disturbances. Figure 17 presents the PV voltage and power under 5% and 10% degradation of the converter components. The voltage convergence speed slightly increases, but abrupt changes in weather conditions lead to parasitic ripples of 80 mV for 5 % degradation and 240 mV for 10%. The power exhibits slightly larger ripples. These three sets of simulations demonstrate that the proposed controller and the overall system are robust. The system remains stable under ±5% variations of the controller parameters and can tolerate input disturbances or sensor inaccuracies up to 1%. Moreover, the overall performance is only slightly affected by the degradation of the converter components.

The proposed hybrid control structure, combining integral backstepping and SMC, has been designed to ensure real-time implementation while maintaining high robustness against uncertainties and external disturbances. The performed sensitivity and robustness analysis confirms the system's stability and reliability under various conditions, directly supporting the feasibility of practical implementation on a hardware platform. The tuning of the control parameters does not require significant effort, as the gains are derived from explicit analytical relations. Moreover, the control law relies on simple arithmetic operations such as multiplications, additions, and integrations, minimizing the computational load. At a switching frequency of 5 kHz, the total computation time per control period is estimated between 50 and 70 µs, including signal

acquisition, control law computation, and PWM signal update. This duration remains well below the sampling period (200 µs), ensuring reliable real-time execution on modern microcontrollers. The integration of the ANN, consisting of a single hidden layer with 50 neurons, does not significantly increase the computational burden thanks to the optimized number of operations. Evaluating the network per control period requires less than 20 µs additional time, which remains compatible with a 5 kHz sampling frequency. An efficient implementation can therefore be achieved on a DSP or a modern microcontroller, providing the required computing power and precision for real-time processing.

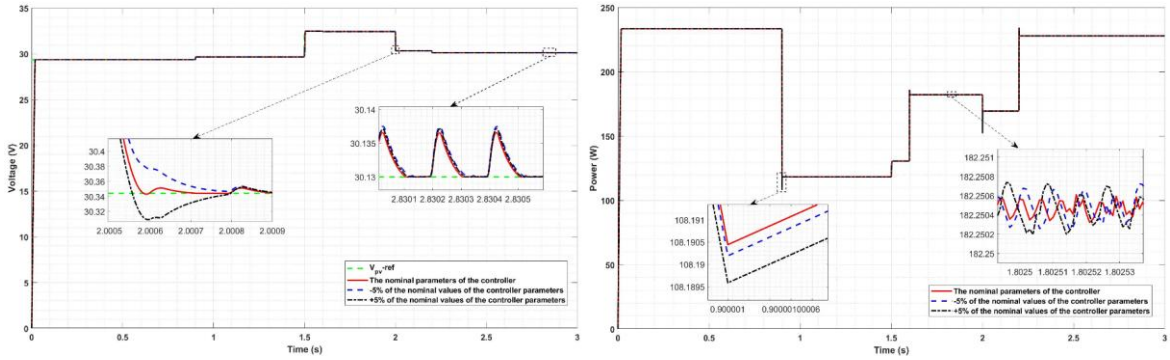


(a) (b)

Figure 15. Sensitivity analysis of the proposed controller with ±5% variation of the controller nominal values: (a) PV module voltage and (b) PV module power

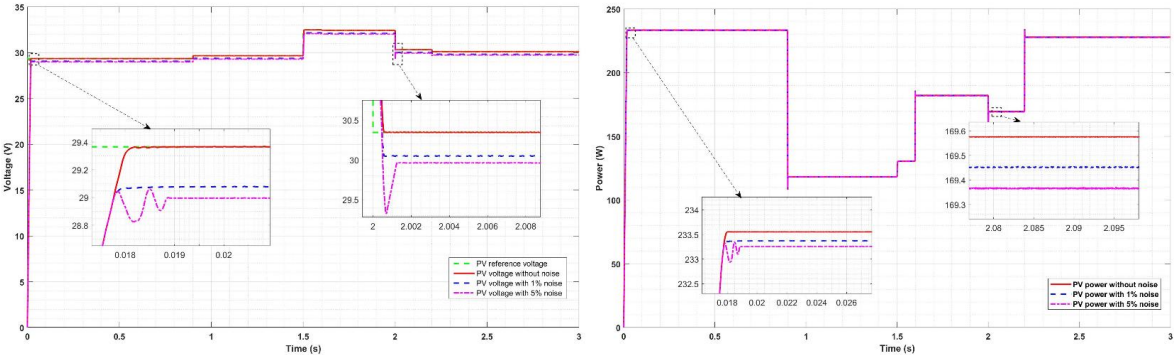


(a) (b)

Figure 16. Robustness analysis of the proposed controller under input disturbances with 1% and 5% noise: (a) PV module voltage and (b) PV module power

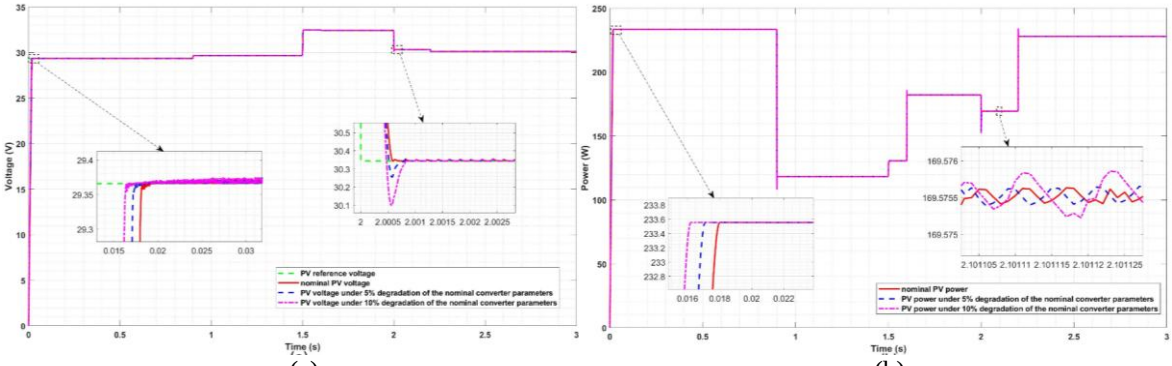


(a) (b)

Figure 17. Robustness analysis of the proposed controller under converter component degradation with 5% and 10% reductions of the nominal component values: (a) PV module voltage and (b) PV module power

Finally, the proposed structure offers promising potential for implementation on real hardware and deployment on an experimental bench or in field conditions, paving the way for future experimental validation. The combination of hybrid control and the ANN, along with the controller's manageable computational load, makes this approach particularly suitable for embedded photovoltaic systems requiring speed, stability, and adaptability.

## 5. CONCLUSION

This paper has presented a hybrid MPPT technique called ANN-IBSMC. This approach combines artificial neural networks with a novel controller that integrates the backstepping technique, its integral component, and SMC. The synergy of these control methods enables near-perfect accuracy (99.996%) by effectively eliminating the error between the actual PV module voltage and the reference voltage provided by the neural network. The strategy also achieves a very fast convergence time, surpassing, on average, ANN-BSMC by 8.3%, ANN-ISMC by 10.32%, and ANN-backstepping by 61.75%. It exhibits a sensitivity margin tolerating ±5% variations in controller parameters, ±1% input disturbances or sensor inaccuracies, as well as a ±5% to ±10% degradation of the converter component values. Furthermore, its computational load remains acceptable, allowing implementation on moderately capable microprocessors. This level of performance ensures highly accurate and rapid tracking of the maximum power point, even under varying weather conditions, thereby enabling a significant increase in electrical energy production, equivalent to several tens of kilowatt-hours for large-scale photovoltaic systems.

## ACKNOWLEDGMENTS

The authors would like to state that this research was not supported by any research grant or contract. This work was carried out as part of the doctoral research conducted at Mohammadia School of Engineers, and the authors would like to thank Mohammadia School of Engineers for providing the academic and institutional framework in which this research was completed.

## FUNDING INFORMATION

This research did not receive any specific grant from funding agencies in the public, commercial, or not-for-profit sectors. The article processing charge was personally covered by the corresponding author.

## AUTHOR CONTRIBUTIONS STATEMENT

This journal uses the Contributor Roles Taxonomy (CRediT) to recognize individual author contributions, reduce authorship disputes, and facilitate collaboration.

| Name of Author | C | M | So | Va | Fo | I | R | D | O | E | Vi | Su | P | Fu |
|---|---|---|---|---|---|---|---|---|---|---|---|---|---|---|
| Naoufal Zhani | ✓ | ✓ | ✓ | ✓ | ✓ | ✓ | ✓ | ✓ | ✓ | ✓ | ✓ | | ✓ | |
| Hassane Mahmoudi | | ✓ | | ✓ | | | ✓ | ✓ | | ✓ | ✓ | ✓ | ✓ | |

C : **C**onceptualization
M : **M**ethodology
So : **So**ftware
Va : **Va**lidation
Fo : **Fo**rmal analysis
I : **I**nvestigation
R : **R**esources
D : **D**ata Curation
O : Writing - **O**riginal Draft
E : Writing - Review & **E**diting
Vi : **Vi**sualization
Su : **Su**pervision
P : **P**roject administration
Fu : **Fu**nding acquisition

## CONFLICT OF INTEREST STATEMENT

Authors state no conflict of interest.

## DATA AVAILABILITY

The data that support the findings of this study are available from the corresponding author, [NZ], upon reasonable request.

## REFERENCES


[1] G. M. Tina, C. Ventura, S. Ferlito, and S. De Vito, "A state-of-art-review on machine-learning based methods for PV," *Applied Sciences*, vol. 11, no. 16, p. 7550, Aug. 2021, doi: 10.3390/app11167550.

[2] V. Jately, B. Azzopardi, J. Joshi, B. Venkateswaran V, A. Sharma, and S. Arora, "Experimental analysis of hill-climbing MPPT algorithms under low irradiance levels," *Renewable and Sustainable Energy Reviews*, vol. 150, p. 111467, Oct. 2021, doi: 10.1016/j.rser.2021.111467.

[3] H. Abouobaida, Y. Mchaouar, Y. Abouelmahjoub, H. Mahmoudi, A. Abbou, and M. Jamil, "Performance optimization of the INC-COND fuzzy MPPT based on a variable step for photovoltaic systems," *Optik*, vol. 278, p. 170657, May 2023, doi: 10.1016/j.ijleo.2023.170657.

[4] A. Belhadj Djilali, A. Yahdou, H. Benbouhenni, and I. Colak, "Improved incremental conductance MPPT technique designed to addressing drift problem in a photovoltaic system," *Electric Power Components and Systems*, pp. 1–14, May 2024, doi: 10.1080/15325008.2024.2348040.

[5] H. Rizki, E.-M. Boufounas, A. El Amrani, M. El Amraoui, and L. Bejjit, "Performance enhancement of a solar photovoltaic system with differential evolution-optimized quasi sliding mode control," *E3S Web of Conferences*, vol. 601, p. 00064, Jan. 2025, doi: 10.1051/e3sconf/202560100064.

[6] A. Boussafa, R. Rabeh, M. Ferfra, and K. Chennoufi, "Experimental test of optimizing maximum power point tracking performance in solar photovoltaic arrays based on backstepping control and optimized by genetic algorithm," *Results in Engineering*, vol. 23, p. 102746, Sep. 2024, doi: 10.1016/j.rineng.2024.102746.

[7] Z. Yan, Z. Miyuan, W. Yajun, C. Xibiao, and L. Yanjun, "Photovoltaic MPPT algorithm based on adaptive particle swarm optimization neural-fuzzy control," *Journal of Intelligent & Fuzzy Systems*, vol. 44, no. 1, pp. 341–351, Jan. 2023, doi: 10.3233/JIFS-213387.

[8] H. S. Agha, Z. Koreshi, and M. B. Khan, "Artificial neural network based maximum power point tracking for solar photovoltaics," in *2017 International Conference on Information and Communication Technologies (ICICT)*, Dec. 2017, pp. 150–155. doi: 10.1109/ICICT.2017.8320180.

[9] A. A. Al-Samawi, A. S. Atiyah, and A. H. Al-Jrew, "Power optimization of partially shaded PV system using interleaved boost converter-based fuzzy logic method," *Eng*, vol. 6, no. 8, p. 201, Aug. 2025, doi: 10.3390/eng6080201.

[10] N. Zhani and H. Mahmoudi, "Comparison of the performance of MPPT control techniques (fuzzy logic, incremental conductance and perturb & observe) under MATLAB/Simulink," *IFAC-PapersOnLine*, vol. 58, no. 13, pp. 617–623, 2024, doi: 10.1016/j.ifacol.2024.07.551.

[11] H. Alhusseini, L. M. Abdali, H. A. Issa, and V. I. Velkin, "Adaptive particle swarm optimization based model predictive control MPPT algorithm for PV systems under partial shading conditions," *Results in Engineering*, vol. 28, p. 107419, Dec. 2025, doi: 10.1016/j.rineng.2025.107419.

[12] A. O. Baatiah, A. M. Eltamaly, and M. A. Alotaibi, "Improving photovoltaic MPPT performance through PSO dynamic swarm size reduction," *Energies*, vol. 16, no. 18, p. 6433, Sep. 2023, doi: 10.3390/en16186433.

[13] S. A. Bonab, W. Song, and M. Yazdani-Asrami, "Physics-informed neural network model for transient thermal analysis of superconductors," *Superconductor Science and Technology*, vol. 38, no. 8, p. 08LT01, Aug. 2025, doi: 10.1088/1361-6668/adf3eb.

[14] A. M. A. Malkawi *et al.*, "Maximum power point tracking enhancement for PV in microgrids systems using dual artificial neural networks to estimate solar irradiance and temperature," *Results in Engineering*, vol. 25, p. 104275, Mar. 2025, doi: 10.1016/j.rineng.2025.104275.

[15] J. de D. Nguimfack-Ndongmo, A. Harrison, N. H. Alombah, R. Kuate-Fochie, D. Ajesam Asoh, and G. Kenné, "Adaptive terminal synergetic-backstepping technique based machine learning regression algorithm for MPPT control of PV systems under real climatic conditions," *ISA Transactions*, vol. 145, pp. 423–442, Feb. 2024, doi: 10.1016/j.isatra.2023.11.040.

[16] K. Abdouni, H. Ennasri, A. Drighil, H. Bahri, M. Bour, and M. Benboukous, "Efficient and robust nonlinear control MPPT based on artificial neural network for PV system," *International Journal of Power Electronics and Drive Systems (IJPEDS)*, vol. 15, no. 3, p. 1914, Sep. 2024, doi: 10.11591/ijpeds.v15.i3.pp1914-1924.

[17] H. Rizki, F. E. Lamzouri, E.-M. Boufounas, A. El Amrani, and L. Bejjit, "Advanced global MPPT strategy for PV systems using high-order sliding mode control, ABC optimization, and neural network prediction under partial shading conditions," *Computers and Electrical Engineering*, vol. 127, p. 110562, Oct. 2025, doi: 10.1016/j.compeleceng.2025.110562.

[18] M. Yılmaz, A. Kaleli, and M. F. Çorapsız, "Machine learning based dynamic super twisting sliding mode controller for increase speed and accuracy of MPPT using real-time data under PSCs," *Renewable Energy*, vol. 219, p. 119470, Dec. 2023, doi: 10.1016/j.renene.2023.119470.

[19] H. Doubabi, I. Salhi, M. Chennani, and N. Essounbouli, "High performance MPPT based on TS fuzzy–integral backstepping control for PV system under rapid varying irradiance—experimental validation," *ISA Transactions*, vol. 118, pp. 247–259, Dec. 2021, doi: 10.1016/j.isatra.2021.02.004.

[20] K. Ali *et al.*, "Robust integral backstepping based nonlinear MPPT control for a PV system," *Energies*, vol. 12, no. 16, p. 3180, Aug. 2019, doi: 10.3390/en12163180.

[21] D. Xu, G. Wang, W. Yan, and X. Yan, "A novel adaptive command-filtered backstepping sliding mode control for PV grid-connected system with energy storage," *Solar Energy*, vol. 178, pp. 222–230, Jan. 2019, doi: 10.1016/j.solener.2018.12.033.

[22] B. Torchani *et al.*, "Adaptive sliding mode control based on maximum power point tracking for boost converter of photovoltaic system under reference voltage optimizer," *Frontiers in Energy Research*, vol. 12, Oct. 2024, doi: 10.3389/fenrg.2024.1485470.

[23] R. EL Idrissi, A. Abbou, and M. Salimi, "Artificial neural-network-based maximum power point tracking for photovoltaic pumping system using backstepping controller," in *2018 IEEE 59th International Scientific Conference on Power and Electrical Engineering of Riga Technical University (RTUCON)*, Nov. 2018, pp. 1–7. doi: 10.1109/RTUCON.2018.8659808.

[24] C. C. Ahmed, M. Cherkaoui, and M. Mokhlis, "MPPT control for photovoltaic system using hybrid method under variant weather condition," in *2019 International Conference on Wireless Technologies, Embedded and Intelligent Systems (WITS)*, Apr. 2019, pp. 1–5. doi: 10.1109/WITS.2019.8723854.

[25] E. idrissi Rafika, A. Abbou, M. Mohcine, and M. Salimi, "A comparative study of MPPT controllers for photovoltaic pumping system," in *2018 9th International Renewable Energy Congress (IREC)*, Mar. 2018, pp. 1–6. doi: 10.1109/IREC.2018.8362524.

[26] A. Taouni, A. Abbou, M. Akherraz, A. Ouchatti, and R. Majdoul, "MPPT design for photovoltaic system using backstepping control with boost converter," in *2016 International Renewable and Sustainable Energy Conference (IRSEC)*, Nov. 2016, pp. 469–475. doi: 10.1109/IRSEC.2016.7983920.
[27] M. Mokhlis, M. Ferfra, H. A. Vall, R. El Idrissi, C. C. Ahmed, and A. Taouni, "Comparative study between the different MPPT techniques," in *2020 5th International Conference on Renewable Energies for Developing Countries (REDEC)*, Jun. 2020, pp. 1–6. doi: 10.1109/REDEC49234.2020.9163591.
[28] K. Boudaraia, H. Mahmoudi, and A. Abbou, "MPPT design using artificial neural network and backstepping sliding mode approach for photovoltaic system under various weather conditions," *International Journal of Intelligent Engineering and Systems*, vol. 12, no. 6, pp. 177–186, Dec. 2019, doi: 10.22266/ijies2019.1231.17.
[29] H. Yatimi, Y. Ouberri, and E. Aroudam, "Enhancement of power production of an autonomous PV system based on robust MPPT technique," *Procedia Manufacturing*, vol. 32, pp. 397–404, 2019, doi: 10.1016/j.promfg.2019.02.232.
[30] E. Kabalci and A. Boyar, "Highly efficient interleaved solar converter controlled with extended Kalman filter MPPT," *Energies*, vol. 15, no. 21, p. 7838, Oct. 2022, doi: 10.3390/en15217838.
[31] I. El Haji, M. Megrini, M. Kchikach, S. Sahbani, A. Gaga, and A. El Hasnaoui, "Performance optimization of symmetrical multi-level boost converter using hybrid MPPT-ANN for solar energy applications," *Results in Engineering*, vol. 26, p. 104729, Jun. 2025, doi: 10.1016/j.rineng.2025.104729.
[32] S. Albert Alexander, R. Harish, M. Srinivasan, and D. Sarathkumar, "Power quality improvement in a solar PV assisted microgrid using upgraded ANN-based controller," *Mathematical Problems in Engineering*, vol. 2022, pp. 1–12, Oct. 2022, doi: 10.1155/2022/2441534.

## BIOGRAPHIES OF AUTHORS

**Naoufal Zhani** is a Ph.D. candidate in electrical engineering at the Mohammadia School of Engineers, Rabat, Morocco. He received his bachelor's degree in electronics, electrotechnics and automation in 2017, and his master's degree in embedded systems in 2020, both from Abdelmalek Essaâdi University, Morocco. His research focuses on the optimization of photovoltaic energy conversion chains, automation, and control of power systems. He is particularly interested in enhancing the efficiency and robustness of PV systems under changing environmental conditions through the development of advanced control strategies. He can be contacted at email: zhani.naoufal@research.emi.ac.ma.

**Hassane Mahmoudi** received a B.S. degree in electrical engineering from Mohammadia School of Engineers, Rabat, Morocco, in 1982, and a Ph.D. degree in power electronics from Montefiore Institute of Electrical Engineering, Luik, Belgium, in 1990. He was an assistant professor of physics at the Faculty of Sciences, Meknes, Morocco, from 1982 to 1990. Since 1992, he has been a professor at the Mohammadia School of Engineers, Rabat, Morocco. He was the head of the Electric Engineering Department for four years (1999, 2000, 2006, and 2007), and the deputy director in charge of Research and Cooperation between 2019 and 2022. Since 2022, he has held the Director position of Mohammadia School of Engineers. His research interests include static converters, electrical motor drives, active power filters, and electromagnetic compatibility. He can be contacted at email: mahmoudi@emi.ac.ma.